Single-chip electron spin resonance detectors operating at 50 GHz, 92 GHz, and 146 GHz

Jeong, Minki

DOI:
10.1016/j.jmr.2017.03.013

Document Version
Peer reviewed version

Citation for published version (Harvard):
Jeong, M 2017, 'Single-chip electron spin resonance detectors operating at 50 GHz, 92 GHz, and 146 GHz', Journal of Magnetic Resonance, vol. 278, pp. 113-121. https://doi.org/10.1016/j.jmr.2017.03.013

Journal of Magnetic Resonance **XXX**, YYYYYY (2017)

Single-chip electron spin resonance detectors operating at 50 GHz, 92 GHz, and 146 GHz

Alessandro V. Matheoud[1], Gabriele Gualco[1], Minki Jeong[1], Ivica Zivkovic[1], Jürgen Brugger[1], Henrik M. Rønnow[1], Jens Anders[2], and Giovanni Boero [1, a)]

[1]*Ecole Polytechnique Fédérale de Lausanne (EPFL), Lausanne, CH-1015, Switzerland*

[2]*University of Ulm, D-89081 Ulm, Germany*

[a)]*giovanni.boero@epfl.ch*

We report on the design and characterization of single-chip electron spin resonance (ESR) detectors operating at 50 GHz, 92 GHz, and 146 GHz. The core of the single-chip ESR detectors is as integrated LC-oscillator, formed by a single turn aluminum planar coil, a metal-oxide-metal capacitor, and two metal-oxide-semiconductor field effect transistors used as negative resistance network. On the same chip, a second, nominally identical, LC-oscillator together with a mixer and an output buffer are also integrated. Thanks to the slightly asymmetric capacitance of the mixer inputs, a signal at few hundreds MHz is obtained at the output of the mixer. The mixer is used for frequency down-conversion, with the aim to obtain an output signal at a frequency easily manageable off-chip. The coil diameters are 120 μm, 70 μm, and 45 μm for the U-band, W-band, and the D-band oscillators, respectively. The experimental phase noise at 100 kHz offset from the carrier are 90 Hz/Hz$^{1/2}$, 300 Hz/Hz$^{1/2}$, and 700 Hz/Hz$^{1/2}$ at 300 K, respectively. The ESR spectra are obtained by measuring the frequency variations of the single-chip oscillators as a function of the applied magnetic field. The experimental spin sensitivities, as measured with a sample of α,γ-bisdiphenylene-β-phenylallyl (BDPA)/benzene complex, are 1×10^{8} spins/Hz$^{1/2}$, 4×10^{7} spins/Hz$^{1/2}$, 2×10^{7} spins/Hz$^{1/2}$ at 300 K, respectively. We also show the possibility to perform experiments up to 360 GHz by means of the higher harmonics in the microwave field produced by the integrated single-chip LC-oscillators.

1. Introduction

Methods based on the electron spin resonance (ESR) phenomenon are used to investigate samples in a wide temperature range, ranging from above 1000 K [1-4] to below 1 K [5-7]. The measurements are usually performed using relatively large microwave cavities as well as with miniaturized conductive [8-19] or superconducting [7, 20-25] resonators. Miniaturized resonators are typically used in order to maximize the signal-to-noise ratio in experiments with small samples. Purely inductive methods based on microresonators have sensitivities at the level of few hundreds of electrons spins/Hz$^{1/2}$ at low temperatures [7, 19]. Non-inductive techniques can achieve single electron spin sensitivity [26-28] but are generally considered to be less versatile than those based on the more conventional inductive approach [7, 19].

In Refs.[12-15] we presented single-chip integrated inductive ESR detectors, fabricated using complementary metal oxide semiconductor (CMOS) technologies, operating between 8 GHz and 28 GHz in the temperature range from 300 K down to 4 K. The ESR phenomenon was detected as a variation of the frequency of an integrated LC-oscillator due to an effective variation of its coil impedance caused by the resonant complex susceptibility of the sample. Here, we report on the design and characterization of single-chip ESR detectors based on the same operating principle but operating at significantly higher frequency, in particular at 50 GHz (U-band), 92 GHz (W-band), and 146 GHz (D-band). Operation at higher frequency is interesting for several reasons including a potentially better spin sensitivity, a better spectral resolution for some classes of samples, and the access to samples with large zero-field splitting which are "silent" at lower frequency [29-33]. The interesting and the problematic aspects of single-chip ESR detectors with respect to more conventional microresonator based approaches are discussed in details in Sects. 3-5.

2. Operating principle of the single-chip ESR detector

The principle of operation of the single-chip ESR detectors described in this paper is identical to that reported in Refs.[12-15]. In typical experimental conditions, the oscillation frequency of an LC-oscillator coupled with an ensemble of electron spins is given by [13]

$$\omega_{LC\chi} \cong \frac{\omega_{LC}}{\sqrt{1+\eta\chi'}} \tag{1}$$

where

$$\chi' = -\frac{1}{2}\frac{\left(\omega_{LC\chi}-\omega_0\right)T_2^2}{1+T_2^2\left(\omega_{LC\chi}-\omega_0\right)^2+\gamma_e^2B_1^2T_1T_2}\omega_0\chi_0 \tag{2}$$

is the imaginary part of the magnetic susceptibility, $\omega_{LC}=1/\sqrt{LC}$ is the unperturbed oscillator frequency, B_0 is the static magnetic field, $\omega_0=\gamma_eB_0$ is the Larmor frequency, χ_0 is the static magnetic susceptibility, η is the filling factor, γ_e is the electron gyromagnetic ratio, B_1 is the microwave magnetic field, T_1 and T_2 are the relaxation times. In condition of negligible saturation (i.e., for $\gamma_e^2B_1^2T_1T_2<<1$) and for $\eta\chi'<<1$, the peak-to-peak variation of the oscillator frequency is given by

$$\Delta f_{LC} \cong (1/4)\, f_{LC}^2T_2\eta\chi_0 \tag{3}$$

where $f_{LC}=\omega_{LC}/2\pi$ is the oscillator frequency (in Hz). The filling factor η can be written as

$$\eta = \frac{\int_{V_s}\left|B_{u,xy}\right|^2dV}{\int_V\left|B_u\right|^2dV} = \frac{\int_{V_s}\left|B_{u,xy}\right|^2dV}{\mu_0L} \tag{4}$$

where $B_{u,xy}$ is the field produced by a unitary current in the coil (in T/A) in the direction perpendicular to the static magnetic field B_0, V is the entire space where B_u is not zero, and L is the inductance of the coil. The magnetic field produced by the single turn planar coil used in this work is highly inhomogeneous. Consequently, the filling

factor must be, in general, computed numerically using, e.g., the Biot-Savart law [34, 35]. However, numerical simulations show that for samples placed in close proximity (less than 10% coil diameter) to the coil and having a thickness smaller than the coil radius and a width smaller than the coil diameter *d*, the filling factor is, within an error of about $\pm 25\%$, given by

$$\eta \cong \frac{\left|B_u(0,0,0)\right|^2}{\mu_0 L} V_s \cong \frac{V_s}{d^3} \tag{5}$$

The spin sensitivity (given in spins/Hz$^{1/2}$) of an ESR detector can be defined as $N_{\min} = (3N_S / SNR)$, where N_S is the number of spins in the sample and *SNR* is the signal-to-noise ratio (where the noise is expressed as its spectral density in Hz/Hz$^{1/2}$). If we assume that the frequency noise of the oscillator is entirely due to the thermal noise of the coil resistance (i.e., we neglect all other noise sources, in particular the flicker noise and the thermal noise of the transistors), the frequency noise spectral density (in Hz/Hz$^{1/2}$) is $\sqrt{S_\nu} = \sqrt{kTR}(f_{LC} / V_0)$, where V_0 is the oscillation amplitude, R is the coil resistance, and f_0 is the working frequency [18].

3. Description of the single-chip ESR detectors

The three single-chip ESR detectors described in this work were manufactured using a standard 40 nm bulk-CMOS technology (Taiwan Semiconductor Manufacturing Company (TSMC), Taiwan). The use of a 40 nm technology, instead of the 130 nm or 180 nm technologies previously adopted [12, 13, 15], is essential to be able to realize oscillators operating above 100 GHz, with realistic possibilities to achieve operating frequencies and above 300 GHz [36]. Each detector has a size of about 0.6x0.6 mm^2 (see Fig.1) and it is composed of two LC-oscillators, a mixer, and an output buffer (Figs. 1 and 2).

Each LC-oscillator consists of two minimum-length nMOS cross-coupled transistors and an LC-resonator (Fig. 2b). The adoption of nMOS rather than pMOS transistors for the cross-coupled transistor is due to their higher speed [37]. No tail current is required in this topology as the circuit is fed by means of an external power supply. That is important to ensure a reasonable headroom voltage for oscillators based on deep sub-micrometer technologies as well as to avoid additional flicker noise up-conversion from the tail transistor [38]. The U-band and the W-band oscillators have, in parallel with the single-turn planar coil, a pair of integrated metal-oxide-metal (MoM) capacitors having nominal values of 50 fF and 15 fF. The D-band oscillator has no capacitance in parallel with the single-turn planar coil and, hence, the oscillation frequency is determined by the parasitic capacitances, mainly due to the cross-coupled MOS transistors. The geometrical details, the power consumption, the measured frequency noise (FN), the estimation of the minimum microwave magnetic field B_1 at the center of the integrated single-turn planar coil as well as other key features of the integrated oscillators are reported in Table 1. The lower limit in the value of B_1 is determined by the minimum transconductance of the cross-coupled transistor pair required for stable oscillation whereas the upper limit is given by the maximum voltage swing which can be applied across the transistors without damaging their thin gate oxide. The value of B_1 generated by our single-chip detector is estimated by measuring the voltage at the oscillator bias node V_{Idc}. In condition of

stable oscillation [39] the oscillation amplitude is approximately given by $V_0 \cong V_{Idc}$. Hence, $B_1 \cong (1/2)B_u(V_{Idc}/\omega_{LC}L)$, where $B_u \cong \mu_0/d$, d is the coil diameter, and L is the coil inductance. This B_1 estimation is in agreement with saturation experiments with samples of known relaxation times.

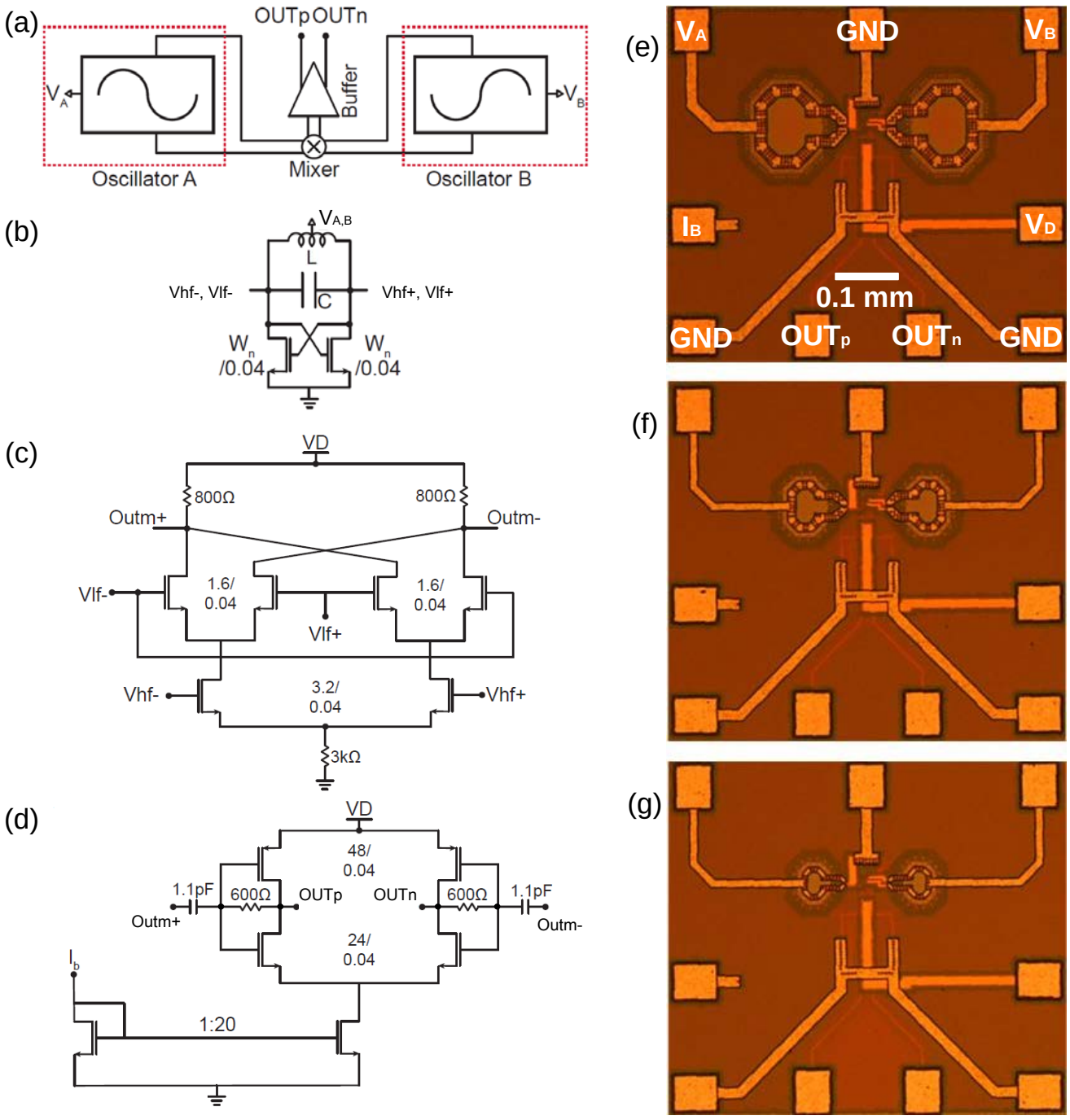

Fig. 1. Detailed schematics of the integrated electronics in the single-chip ESR detectors: (a) Block diagram; (b) LC-oscillator, (c) mixer; (d) output buffer. The dimensions (width/length) of the transistors are in micrometers. Pictures of the single-chip ESR detectors: (e) U-band oscilllator operating at 50 GHz (120 μm diameter coil), (f) W-band oscillator operating at 90 GHz (70 μm diameter coil), (g) D-band oscillator operating at 150 GHz (45 μm diameter coil).

The mixer is a double-balanced Gilbert cell (Fig. 2c), biased with a resistor to ground since simulations revealed that is an efficient way to reduce the corresponding flicker noise. The power consumption associated to such a system depends on the oscillation amplitude through the V_{gs} of each switching transistor, and it can be minimized by reducing the oscillator voltage supply. In order to reduce the capacitive load mismatch between the two oscillators, the two lower switches are double sized transistors with respect to the other four.

The output buffer is a differential class-AB amplifier (self-biased inverter) whose power consumption is controlled by means of an off-chip resistor placed on the PCB. The same mixer and output buffer are used for all detectors. The power consumption of the mixer and the output buffer is about 130 μW (1.3 V, 100 μA).

	U	W	D
Frequency [GHz]	49.2 49.8	90 92	142 146
Coil diameter [μm]	120	70	45
Coil wire width [μm]	15	10	5
Approx. effective inductance [pH]	160	90	65
Approx. effective capacitance [fF]	65 64	35 33	20 18
MOS width [μm]	13.0	13.0	9.6
MOS length [nm]	40	40	40
I_{min} [mA] V_{min} [V] @ 300 K	1.9 0.5	2.5 0.6	2.9 0.7
I_{min} [mA] V_{min} [V] @ 10 K	0.6 0.4	0.8 0.5	0.9 0.5
$B_{1,min}$ [G] @ 300 K	1	2	4
$B_{1,min}$ [G] @ 10 K	2	4	7
FN [Hz/Hz$^{1/2}$] @ 1 kHz, 300 K	900 (3)	2300 (6)	8000 (9)
FN [Hz/Hz$^{1/2}$] @ 10 kHz, 300 K	300 (3)	1100 (6)	2100 (9)
FN [Hz/Hz$^{1/2}$] @ 100 kHz, 300 K	90 (3)	300 (6)	700 (9)
FN [Hz/Hz$^{1/2}$] @ 1 MHz, 300 K	40 (3)	110 (6)	290 (9)
N_{min} [spins/Hz$^{1/2}$] @ 100 kHz, 300 K	1×10^{8} (2×10^{6})	4×10^{7} (5×10^{5})	2×10^{7} (3×10^{4})

Tab1e 1. Key-features of the three single-chip ESR detectors. In the last two rows the theoretical (in parenthesis) and experimentally measured frequency noise and spin sensitivity are compared. The theoretical values are computed, using the equation given in Sect. 2, assuming as noise source only the thermal noise of the single-turn planar coil resistance (about 0.8, 0.9, and 1.3 Ohms) at the given oscillation amplitude (about 0.9 V, 1.1 V, 1.5 V) for the for the 50, 90, and 146 GHz oscillators, respectively. The spin sensitivity is measured (and computed) with a sample of BDPA (spin density: 1.5×10^{27} spins/m^3, relaxation times: $T_1 \cong T_2 \cong 100$ ns) at 300 K [40-42].

As shown in Table 1, the measured frequency noise at 100 kHz from the carrier is up to two orders of magnitude larger than the thermal noise limit due to the coil resistance (see Sect. 2). This is mainly due to a very large *1/f* frequency noise having corner frequency above 1 MHz from the carrier. The combination of an excessively large B_1 (for samples with a large T_1T_2 value) and the *1/f* noise are responsible for the very significant

deterioration of the spin sensitivity (two to three orders of magnitude) with respect to the thermal noise limit reported in Table 1 (and discussed in Sect. 5).

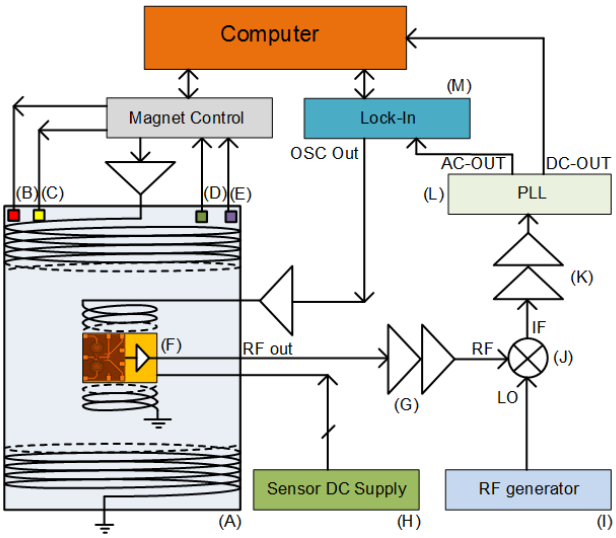

Fig. 3. Block diagram of the complete set-up. (A) Oxford Superconducting Magnet 0-17 T with variable temperature insert, (B) helium-flux valve; (C) heater; (D) B_0 meter; (E) thermometer; (F) single-chip ESR detector with off-chip buffer (TI-THS4304); (G) RF amplification stage, composed of two HMC-C001, 15 dB gain each); (H) DC power supply (Keysight E3631A, Keithley 2400); (I) RF generator (Stanford Research Systems SG384); (J) Mixer (Mini-Circuits ZFM-2000+); (K) IF amplification stage (two Mini-Circuits ZFL-500LN, 24 dB gain each); (M) Homemade low-noise Phase-Locked-Loop (200 kHz FM bandwidth, 150-200 MHz lock range) based on a phase detector (HMC439QS16G) and a local oscillator (Crystek CVCO55CL-0150-0200); (M) Lock-in amplifier (EG&G 7260).

Figure 3 shows the block diagram the complete set-up used to perform the electron spin resonance experiments reported in this work. In order to provide 50 Ω driving capability, an off-chip non-inverting 6 dB buffer amplifier is mounted on a printed circuit board at a few mm from the single-chip ESR detector. Its power consumption is about 85 mW (±2.5 V, ±17 mA) at room temperature and about 30 mW (±1.8 V, ±8 mA) at cryogenic temperatures. Field modulation with lock-in synchronous demodulation is used as in conventional continuous wave ESR spectroscopy. The field modulation coil produces a maximum field modulation of about 2 G at 100 kHz. The signal at the output of the off-chip buffer amplifier is further down-converted to a second intermediate frequency (150-200 MHz) to match the lock range of a homemade frequency-to-voltage converter based on a phase-locked-loop (PLL). The latter produces two output signals: (1) an “AC-ESR signal” carrying the information on the frequency modulation of the integrated oscillator due to the field modulation, and (2) a “DC-ESR signal” containing the information about the frequency difference between the two integrated oscillators. The AC-ESR signal is subsequently demodulated using a lock-in amplifier whereas the DC-ESR signal is directly acquired. In some measurements with samples having very broad lines, the field modulation is not used and only the DC-ESR signal is measured.

4. Electron spin resonance experiments

Figures 4, 5, 6 show the results of measurements performed with the three single chip ESR detectors operating at 50, 92, and 146 GHz, respectively. We performed experiments on samples having very different characteristics, including an exchange narrowed standard system (BDPA), two hyperfine splitted systems having 100% and 1% concentrations (Cu^{2+} in TPP and in $Ni(mnt)_2$), a zero field splitted system (Cr_3^+ in Al_2O_3), and a quantum magnet with a very broad line in its paramagnetic state (SCBO). This variety of samples helps in underlining both the interesting and the problematic aspects of the single-chip ESR detector approach.

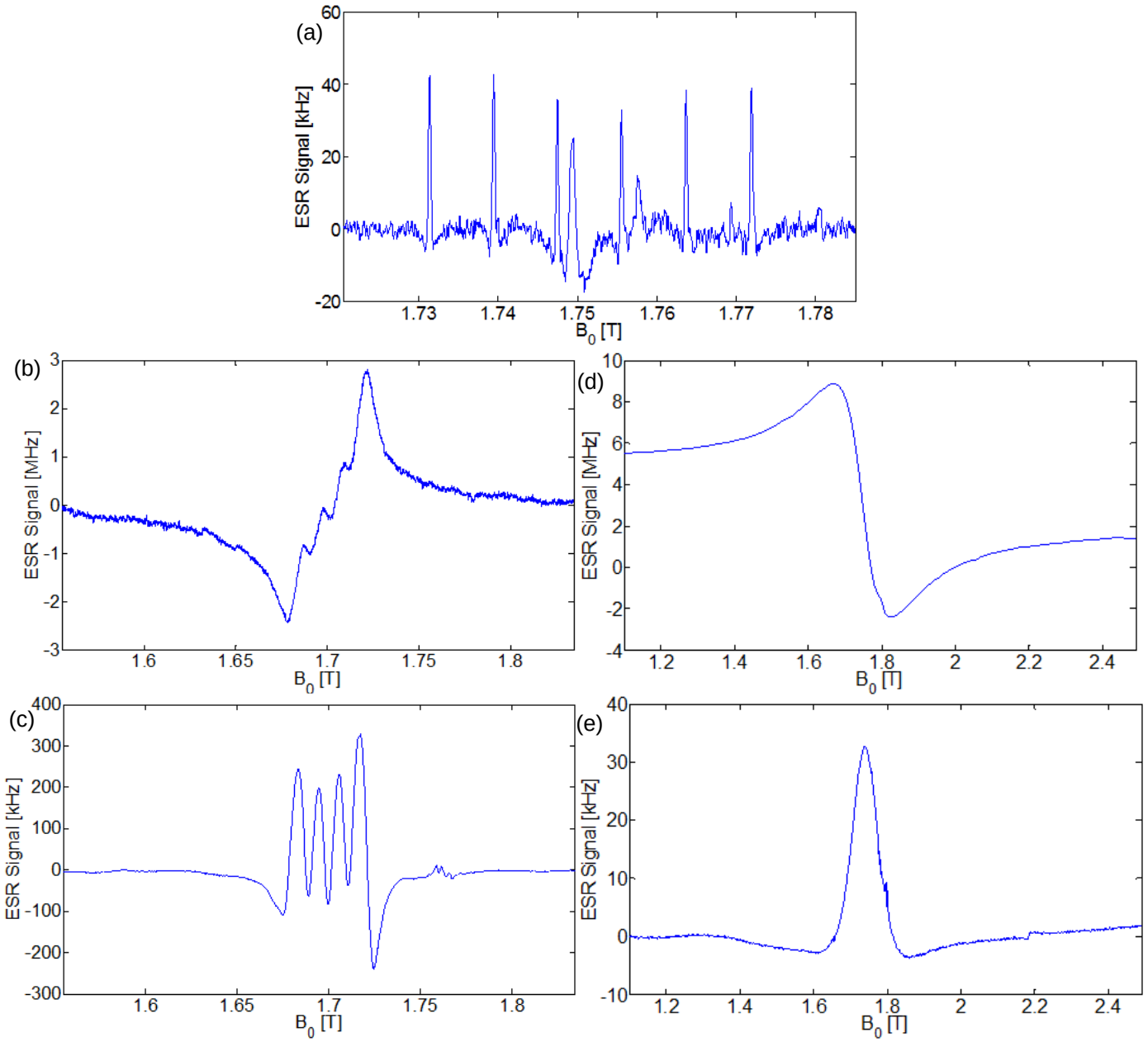

Fig. 4. ESR experiments performed with the 50 GHz single-chip detector. Experimental conditions notations: T is the sample temperature, B_1 is the amplitude of the microwave magnetic field, B_m is the amplitude of the modulation magnetic field, ν_m is the frequency of the magnetic field modulation, t_s is the time interval of the magnetic field sweep, Δf is the equivalent noise bandwidth of the lock-in. (a) ESR spectrum of a $20\times20\times10$ μm^3 sample of Mn:MgO (see text) with ν_m=9.8 kHz, B_m=0.2 mT, $B_1 \cong 0.2$ mT, Δf = 2.5 Hz, T=300 K, t_s=5 min. (b-c) ESR spectra performed of a $60\times60\times60$ μm^3 sample of CuTPP (see text) at T=300 K, (b) DC signal, (c) AC signal with ν_m=9.8 kHz, B_m=0.9 mT, $B_1 \cong 0.2$ mT, Δf = 2.5 Hz, t_s=11 min. (d-e) ESR spectra of a $100\times100\times20$ μm^3 sample of SCBO (see text) at T=100 K, (d) DC signal, (e) AC signal with ν_m=9.8 kHz, B_m=0.15 mT, $B_1 \cong 0.2$ mT, Δf = 0.25 Hz, t_s=28 min.

In Fig. 4 are reported the results of measurements performed using the 50 GHz single-chip oscillator. Fig. 4a shows the spectrum obtained with a powder sample of MgO (98% purity, Sigma Aldrich, 220361) having a volume of about $20\times20\times10\ \mu m^3$. The spectrum consists, mainly, of six hyperfine lines, originated by the $^{55}Mn^{2+}$ ion having nuclear spin I=5/2 (and electron spin S=5/2). The measured separation between the lines is about 8.7 mT, in agreement with previous measurements [43]. The measured width of each hyperfine line is about 0.8 mT for a B_1 of about 0.2 mT, i.e., close to the minimum possible value with our oscillator. Measurements performed using an ordinary cavity at 10 GHz show that the unsaturated linewidth is about 0.2 mT, with significant saturation for B_1 values above 0.05 mT (due to a $T_1 \cong 140$ ns and a $T_2 \cong 33$ ns). At the lowest B_1 possible with our oscillator (i.e., about 0.2 mT), the signal is broadened by a factor of four and reduced in amplitude by a factor of three with respect to a measurement performed with a B_1 below 0.05 mT. The six hyperfine lines are likely to be caused only by (m_s=-1/2, m_s=1/2) transitions. All other transitions are not observed due to their strongly anisotropic character [44], which makes them invisible for a sample in powder form. Assuming a Mn^{2+} of concentration about 0.2% (as estimated for a nominally identical sample in Ref. [45]) and a density of about 3600 kg/m^3 (as for a crystal of MgO, probably an overestimation with respect to the effective grain density), the number of Mn^{2+} spins contained in the sample is about 4×10^{11}. Since the signal amplitude is about 50 kHz and the noise is about 100 Hz/Hz$^{1/2}$, the spin sensitivity (as defined in Sect. 2) is about 2.5×10^9 spins/Hz$^{1/2}$ for this sample. In order to cross-check if the obtained value is coherent with measurements performed on other samples, we can compute a *normalized* spin sensitivity for a S=1/2 spin system having a single unsaturated line of 0.1 mT measured with optimal field modulation, which gives a normalized spin sensitivity of about 5×10^7 spins/Hz$^{1/2}$. A large broader signal is also clearly visible close to the third hyperfine line starting from lower fields, as also reported in Ref. [45] and attributed to unknown additional paramagnetic impurities in the MgO sample. In our case, we also observe an additional broad signal between the fourth and fifth line and further smaller lines, probably caused by other impurities.

In Fig. 4b,c are reported experiments with a single crystal of 5,10,15,20-Tetraphenyl-21*H*,23*H*-porphine Cu^{2+} (CuTPP, Aldrich, 252182) having a volume of $60\times60\times60\ \mu m^3$. The spectrum consists of four hyperfine lines (the ^{63,65}Cu nuclei have spin I=3/2) each having a width of about 10 mT and a separation from the others of about 16 mT. Due to the limited maximum field modulation available in our set-up (about 0.2 mT), the AC-ESR signal (see Fig. 4c) is about one order of magnitude smaller than the DC-ESR signal (see Fig. 4b). CuTPP has a density of about 1400 kg/m^3, a molecular weight of 676 and, hence, a spin density of about 1.2×10^{27} spins/m^3 and a number of Cu^{2+} spins contained in the sample of about 2.7×10^{14} spins. Since the signal amplitude is about 300 kHz and the noise is about 100 Hz/Hz$^{1/2}$, the spin sensitivity for this sample is about 3×10^{11} spins/Hz$^{1/2}$. The *normalized* spin sensitivity considering four hyperfine lines for an unsaturated 0.1 mT line of a S=1/2 system measured with optimal field modulation is about 2×10^7 spins/Hz$^{1/2}$, a value coherent with the one computed with the Mn:MgO sample.

In Figs. 4d,e are reported results obtained on a $100\times90\times20$ μm^3 single crystal of $SrCu(BO_3)_2$, a widely investigated quantum magnet (see, e.g., Ref. [46, 47]), which we have measured its paramagnetic state at 100 K. The spectrum consists of a single broad line (about 170 mT). As for the CuTPP sample, the sub-optimal field modulation amplitude determines an AC-ESR signal (about 30 kHz, see Fig. 4e) much smaller than the DC-ESR signal (about 10 MHz, see Fig. 4d). Despite the larger noise in the DC-ESR signal (about 940 Hz rms with respect to about 130 Hz rms) the signal-to-noise ratio is larger for the DC-ESR signal.

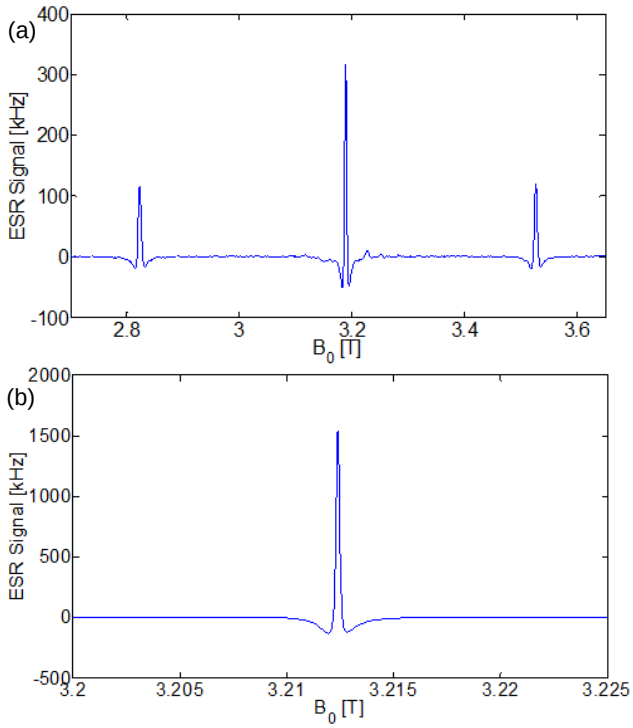

Fig. 5. ESR experiments performed with the 92 GHz single-chip detector. (a) ESR spectra of a $50\times50\times40$ μm^3 sample of ruby (see text) with ν_m =9.8 kHz, B_m =0.15 mT, $B_1 \cong 0.3$ mT, Δf = 0.25 Hz, t_s =18 min, T=200 K; (b) ESR spectra of a $3\times3\times3$ μm^3 μm^3 of BDPA (see text) with ν_m =98 kHz, B_m =0.12 mT, $B_1 \cong 0.25$ mT, Δf = 0.25 Hz, t_s =4.5 min, T=200 K.

Figure 5a shows the results of a measurement performed using the 92 GHz single-chip oscillator on a single crystal of 1% Cr^{3+}:Al_2O_3 (Ruby G10, Saphirwerk Industrieprodukt AG, Switzerland) having a volume of about $50\times50\times40$ μm^3. Only the three high field lines are shown. In Figure 5b are reported the results obtained with a single crystal of BDPA (1:1 α,γ-bisdiphenylene-β-phenylallyl/benzene complex, Sigma Aldrich 152560) having a volume of about $3\times3\times3$ μm^3. Due to the excessive B_1 (about 0.25 mT) and the sub-optimal field modulation amplitude, the signal amplitude is significantly reduced (1.5 MHz instead of 13 MHz) and the linewidth is broadened (0.4 mT instead of 0.1 mT). Assuming a spin density of about 1.5×10^{27} spins/m^3 [42], the total number of spin contained in the sample is about 4×10^{10} spins/m^3. Since the signal amplitude is about 1.5 MHz and the frequency noise spectral density is about 300 Hz/Hz$^{1/2}$, the experimentally achieved spin sensitivity, according to the definition given in Section 2, is about 3×10^7 spins/Hz$^{1/2}$. In Table I are reported the obtained spin sensitivities measured with a BDPA sample using the three single-chip ESR detectors. The large difference (about

two orders of magnitude) between the experimentally achieved spin sensitivity and the thermal noise limit (given in parenthesis) is discussed in details in Sect. 5.

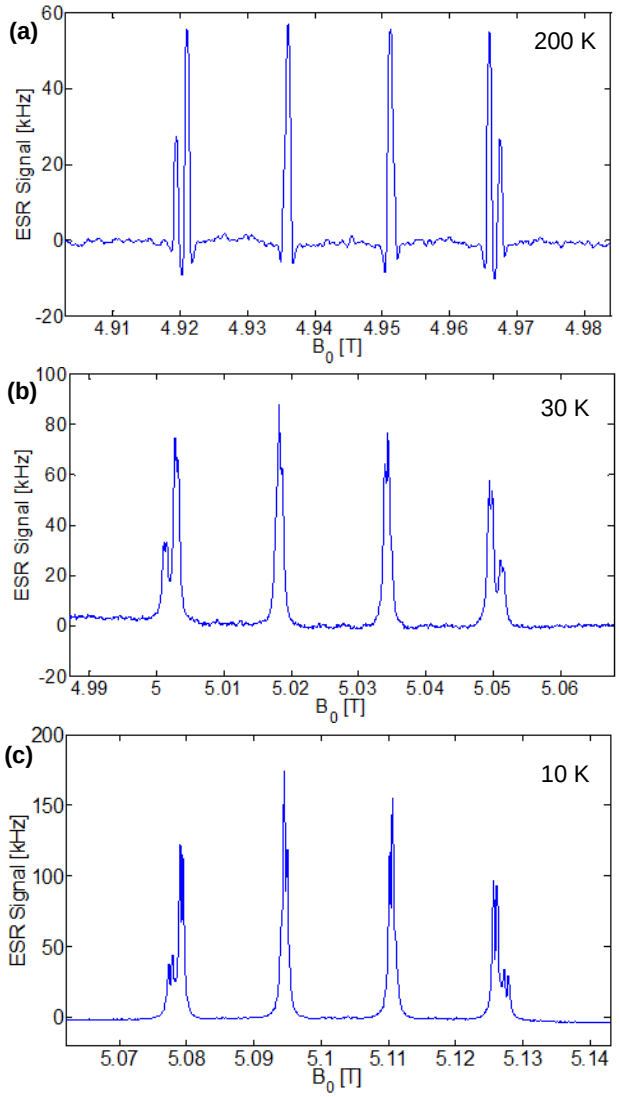

Fig. 6. ESR experiments performed with the 146 GHz single-chip detector. (a-c) ESR spectra of a 40x40x5 μm^3 sample of 1% Cu(II)(mnt)$_2$ in Ni(mnt)$_2$ with ν_m =98 kHz, B_m =0.15 mT , $B_1 \cong 0.6$ mT, Δf = 0.25 Hz, t_s =16 min at (a) 200 K; (b) 30 K; (c) 10 K.

In Fig. 6 are reported the results of measurements performed using the 146 GHz single-chip oscillator on a single crystal of Cu^{2+}-doped tetramethylammonium-bis(maleonitriledithiolate) nickel with a Cu concentration of 1% (1% Cu(mnt)$_2$) in Ni(mnt)$_2$) and a volume of $40\times40\times5$ μm^3. All spectra show the hyperfine splitting produced by the Cu nuclei (^{63}Cu and ^{65}Cu), both having spin I=3/2. The measured spectra have shapes which are temperature dependent, with more resolved lines at low temperature. At room temperature and at 200 K, the shape of the signal is, with good approximation, the first derivative of a dispersion curve (as expected, see Ref. [14, 15]), whereas at low temperature it is no more the case. The reason for this behaviour is unclear. The shift towards higher fields of the resonance at low temperatures is due to the shift towards higher frequency of the oscillator (about 4.5 GHz from 300 K to 10 K). Assuming a spin density of 1.7×10^{25} spins/m^3 (as obtained from data in Ref. [48]), the measured spin sensitivity for this sample is about 1.8×10^9 spins/Hz$^{1/2}$. The *normalized* spin

sensitivity considering eight hyperfine lines with a 0.1 mT width measured with optimal field modulation is about 4×10^{6} spins/Hz$^{1/2}$.

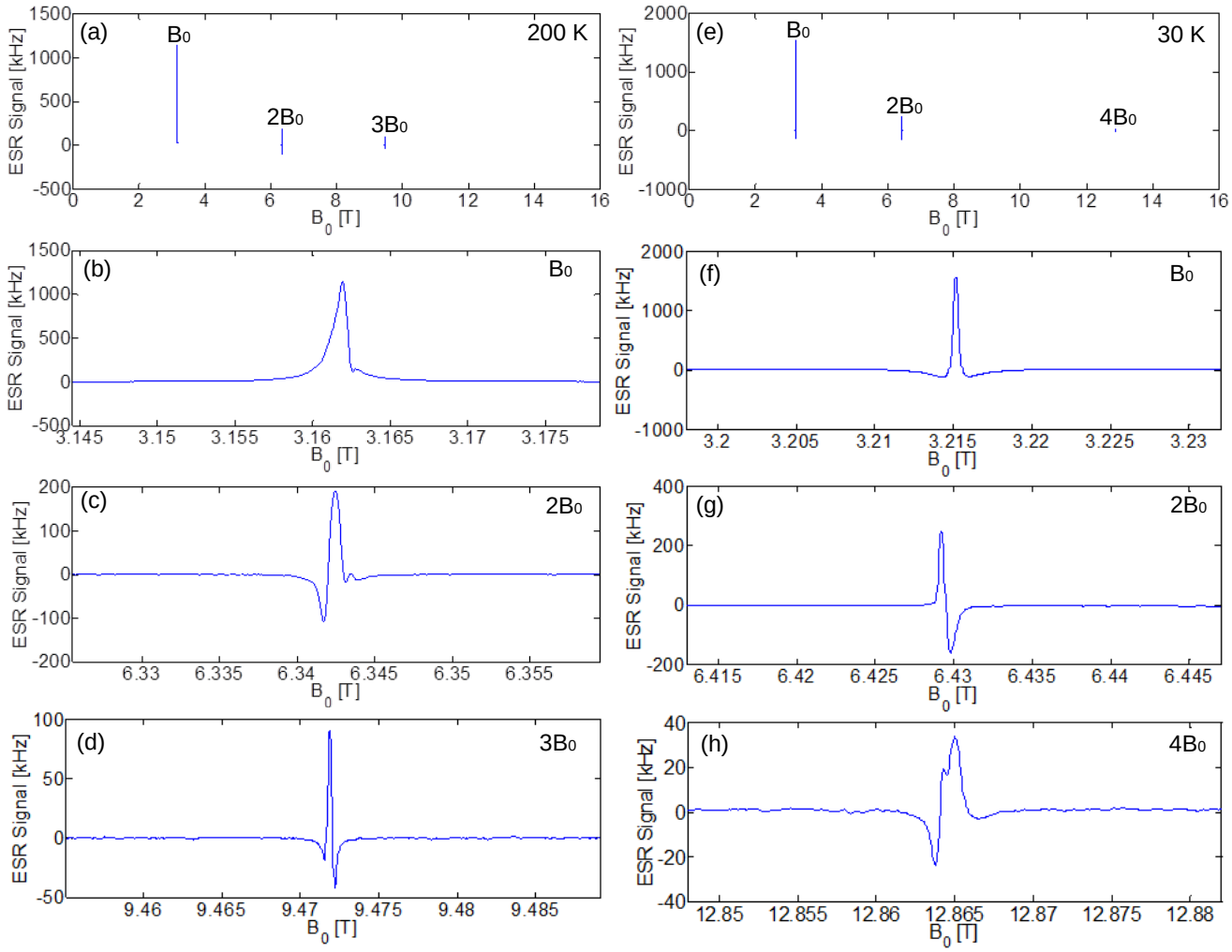

Fig. 7. ESR experiments performed with the 92 GHz single-chip ESR detector with a 6x6x5 μm^3 sample of BDPA at ν_m =98 kHz, B_m =0.12 mT, $B_1 \cong 0.2$ mT, Δf = 0.25 Hz, t_s =3 min (10 mT/min), T=200 K, $\omega_0 \cong 2\pi\times92$ GHz. (a) All measurements. Narrow field sweeps about (b) $B_0 = (\omega_0/\gamma)$, (c) $B_0 = 2(\omega_0/\gamma)$, (d) $B_0 = 3(\omega_0/\gamma)$, respectively. ESR spectra of a 3x3x3 μm^3 of BDPA (see text) with ν_m =98 kHz, B_m =0.12 mT, $B_1 \cong 0.2$ mT, Δf = 0.25 Hz, t_s = 1 min, T=30 K. (e) All measurements. Narrow field sweeps about (f) $B_0 = (\omega_0/\gamma)$, (g) $B_0 = 2(\omega_0/\gamma)$, (h) $B_0 = 4(\omega_0/\gamma)$, respectively. Note: signals at $B_0 = 4(\omega_0/\gamma)$ at 200 K and at $B_0 = 3(\omega_0/\gamma)$ at 30 K have been also observed but not reported in the graphs above because accidentally measured with a much faster magnetic field sweep rate which reduced their signal amplitude and distorted their shape.

Finally, in Fig.7, we show the possibility to perform experiments at higher harmonics of the fundamental frequency of the oscillator. In particular, Fig. 7 shows ESR spectra obtained with a BDPA samples of about 6x6x5 μm^3 and 3x3x3 μm^3. Figure 7a-h show the results of experiments performed at magnetic fields from about 3 T to about 13 T. Resonances are observed at about 3.2, 6.4, 9.5, and 12.9 T. The observed resonant fields correspond to frequencies of about 90, 180, 270, and 360 GHz, which are the fundamental and the second, third, and fourth harmonics of the integrated oscillator. This indicates that the single-chip ESR detectors are capable to perform ESR experiments at least up to the fourth harmonic of the fundamental frequency of the integrated oscillator. Qualitatively we can explain this behavior by the presence of higher harmonics in the oscillator currents and,

hence, in the microwave magnetic field acting on the sample. The signal amplitude significantly decreases at higher harmonics and both the signal shape and its width are dependent on the observed harmonic. The smaller sample is sufficiently small to avoid the transition to the strong coupling regime [13], whereas the larger one is in strong coupling (at the first harmonic but not at the third harmonic). We have attempted to model the experimental results assuming that the sample can be represented by an *RLC* resonator inductively coupled to the *LC*-tank of the integrated oscillator (see details in Ref. [13]). Performing the simulation of the overall electronic circuit using an electronic circuit simulator (in our case Cadence), we obtain that the variation of the fundamental frequency of the oscillator Δf_{LC} is not zero not only when $B_0 \cong (\omega_{LC} / \gamma)$ but also when $B_0 \cong n(\omega_{LC} / \gamma)$, where n is an integer number larger than 1. The simulations predict the observed results with an accuracy well within an order of magnitude in both amplitude and width (the main limitation to the accuracy is presumably in the modelling of the harmonic content in the transistors currents at frequencies close to the cut-off frequency). The reduced sensitivity at higher harmonics (about an order of magnitude for the third harmonic) severely limit the applicability of the higher harmonics of single-chip ESR detectors to high frequency spectroscopy studies of practical interest. Nevertheless, for samples having a sufficiently large signal-to-noise ratio, the possibility to perform multiple-frequency ESR experiments up to 400 GHz with a single detector having a large scale production cost of a few dollars or less is certainly attractive. CMOS [36, 49] or others integrated circuit technologies [50], currently achieving fundamental oscillation frequencies of 300 to 500 GHz, would allow for multiple-frequency ESR experiments up to the THz range.

5. Conclusion and outlook

In this paper we have reported about the design and the performance of three single-chip ESR detectors operating at 50 GHz, 92 GHz, and 146 GHz. Previous designs of single-chip ESR detectors operated up to 28 GHz [12-15]. The higher operating frequency improves the spin sensitivity by more than an order of magnitude. In Table 1 are reported the experimental and theoretical values for the spin sensitivity and the frequency noise spectral density for the three single-chip ESR detectors reported in this work. The measured spin sensitivity is two to three orders of magnitude worse than the one expected if only the thermal noise of the coil resistance is considered. This sensitivity degradation is essentially due to two phenomena: (1) the presence of $1/f$ noise in the frequency noise spectral density up to frequencies as large as 1 MHz from the carrier, and (2) to the large minimum B_1, ranging from 0.2 to 0.7 mT, which causes a significant saturation for samples having T_1T_2 larger than 10^{-19} to 10^{-16} s^2.

Field modulation at frequencies above 1 MHz would help at improving the sensitivity. However, field modulation above 1 MHz and amplitudes above 0.1 mT is not easily implementable, especially at low temperatures, due to heating and T_1-related limitations. The reduction of the 1/f frequency noise is a key issue also for many industrially relevant applications of integrated microwave oscillators [51-54], so it is likely that we will benefit from the advances on this issue of a large community of researchers in industry and academia to improve the spin sensitivity for our specific ESR application.

LC-oscillators with small resonating coils have large microwave fields B_1 ($B_1 \cong I_{DC} Q \mu_0 / d$, where I_{DC} is the oscillator bias current, Q is the quality factor of the *LC*-resonator, and d is the single-turn coil diameter). In order to have stable oscillations, a minimum bias current is required. This, in turns, determines a minimum value for the microwave field B_1 and, hence, a significant saturation for samples having large values of the product T_1T_2 (see above). The use of smaller sensing coil is necessary to reach higher frequencies. This is essentially due to the presence of parasitic capacitances which limit the maximum value of the coil inductance that can be used. Smaller sensing coils produce larger unitary fields and, assuming a similar minimum microwave current as experimentally observed, a larger minimum B_1. The saturation issue can be, in principle, solved by rotating the planar coil axis with respect to the B_0 field direction (usually at 90° for maximum sensitivity). However, this reduces the sensitivity and, consequently, it is a valid approach only for sample having a large signal-to-noise ratio. A possible way out for this saturation issue is to use high electron mobility transistors (HEMT) instead of silicon transistors as elements for the negative feedback of the *LC*-oscillator. The larger electron mobility (more than one order of magnitude at room temperature and more than two order of magnitude at low temperatures) should allow one to have a lower minimum microwave currents to sustain stable oscillations and, hence, lower minimum B_1 fields. Preliminary calculations indicate that HEMT based *LC*-oscillators should allow to obtain B_1 fields of about ten times lower at room temperature (i.e., about 0.01 mT) and more than hundred times lower at low temperatures. Another possible solution to the excessive B_1, would be to use the integrated *LC*-oscillator as local microwave source for a second, co-integrated, *LC*-resonator connected to an amplitude detector (i.e., an

integrated version of a conventional ESR spectrometer). With this approach the B_1 amplitude could be reduced to an arbitrarily low value using an integrated attenuator. Furthermore, this approach would also allow for the implementation of pulsed mode single-chip ESR detectors, where the B_1 field could be pulsed using an integrated switch and the free induction decay or echo signal amplified and downconverted using an integrated microwave amplifier, a mixer, and an IF amplifier, an architecture already demonstrated for NMR spectroscopy at frequencies below 1 GHz [55]. However, this more conventional and versatile approach based on a signal amplitude detection (instead of a frequency detection) requires more complex integrated circuitry and it might not necessarily allow to achieve better spin sensitivity at 10 GHz and above.

As mentioned in the introduction, the use of miniaturized resonators is a valid approach to improve the spin sensitivity for small samples. The single-chip ESR detector contains a miniaturized *LC*-resonator (described in Sect. 3) and, in contrast to the conventional miniaturized resonators, it includes also the microwave source and the most critical part of the detection electronics in a small chip of less than 1 mm^2. The ESR signal at the output of the integrated detector is robustly frequency-encoded. These characteristics make the single-chip ESR detector better suited for operation at very high frequencies (the source, the resonator, and the detector are within a distance of less than 1 mm, de-facto eliminating all concerns about signal-to-noise ratio degradation in the connections) and for their implementation in an array of detectors for simultaneous spectroscopy of several samples in the same magnet. The operation at frequencies above 100 GHz, as demonstrated in this work, is also an important step towards the use of array of single-chip *LC*-oscillators as a low cost alternative to gyrotrons sources in dynamic nuclear polarization (DNP) set-ups. Integrated *LC*-oscillators operating at 300 GHz and 570 GHZ have been already reported [36] and operation at THz frequencies might be possible in the near future. Consequently, the single-chip microwave oscillator approach is suitable for measurements up to the largest magnetic fields currently available.

Acknowledgement

Financial support from the Swiss National Science Foundation is gratefully acknowledged.

References

[1] M.T. Causa, M. Tovar, A. Caneiro, F. Prado, G. Ibanez, C.A. Ramos, A. Butera, B. Alascio, X. Obradors, S. Pinol, F. Rivadulla, C. Vazquez-Vazquez, M.A. Lopez-Quintela, J. Rivas, Y. Tokura, S.B. Oseroff, High-temperature spin dynamics in CMR manganites: ESR and magnetization, Phys Rev B, 58 (1998) 3233-3239.

[2] M. Bakr, M. Akiyama, Y. Sanada, Insitu High-Temperature ESR Measurements for Kerogen Maturation, Org Geochem, 17 (1991) 321-328.

[3] E.M. Decastro, V. Pereira, High Temperature Probe for Epr Measurements, Rev Sci Instrum, 40 (1969) 949.

[4] E. Dormann, D. Hone, V. Jaccarino, High-Temperature Epr in Solid and Molten Paramagnets, Phys Rev B, 14 (1976) 2715-2739.

[5] S. Probst, H. Rotzinger, S. Wunsch, P. Jung, M. Jerger, M. Siegel, A.V. Ustinov, P.A. Bushev, Anisotropic Rare-Earth Spin Ensemble Strongly Coupled to a Superconducting Resonator, Phys Rev Lett, 110 (2013) 157001.

[6] V. Ranjan, G. de Lange, R. Schutjens, T. Debelhoir, J.P. Groen, D. Szombati, D.J. Thoen, T.M. Klapwijk, R. Hanson, L. DiCarlo, Probing Dynamics of an Electron-Spin Ensemble via a Superconducting Resonator, Phys Rev Lett, 110 (2013) 067004.

[7] A. Bienfait, J.J. Pla, Y. Kubo, M. Stern, X. Zhou, C.C. Lo, C.D. Weis, T. Schenkel, M.L.W. Thewalt, D. Vion, D. Esteve, B. Julsgaard, K. Molmer, J.J.L. Morton, P. Bertet, Reaching the quantum limit of sensitivity in electron spin resonance, Nat Nanotechnol, 11 (2016) 253-257.

[8] R. Narkowicz, H. Ogata, E. Reijerse, D. Suter, A cryogenic receiver for EPR, J Magn Reson, 237 (2013) 79-84.

[9] G. Boero, M. Bouterfas, C. Massin, F. Vincent, P.A. Besse, R.S. Popovic, A. Schweiger, Electron-spin resonance probe based on a 100 mu m planar microcoil, Rev Sci Instrum, 74 (2003) 4794-4798.

[10] R. Narkowicz, D. Suter, I. Niemeyer, Scaling of sensitivity and efficiency in planar microresonators for electron spin resonance, Rev Sci Instrum, 79 (2008) 084702.

[11] R. Narkowicz, D. Suter, R. Stonies, Planar microresonators for EPR experiments, J Magn Reson, 175 (2005) 275-284.

[12] J. Anders, A. Angerhofer, G. Boero, K-band single-chip electron spin resonance detector, J Magn Reson, 217 (2012) 19-26.

[13] G. Boero, G. Gualco, R. Lisowski, J. Anders, D. Suter, J. Brugger, Room temperature strong coupling between a microwave oscillator and an ensemble of electron spins, J Magn Reson, 231 (2013) 133-140.

[14] T. Yalcin, G. Boero, Single-chip detector for electron spin resonance spectroscopy, Rev Sci Instrum, 79 (2008) 094105.

[15] G. Gualco, J. Anders, A. Sienkiewicz, S. Alberti, L. Forro, G. Boero, Cryogenic single-chip electron spin resonance detector, J Magn Reson, 247 (2014) 96-103.

[16] Y. Twig, E. Dikarov, A. Blank, Ultra miniature resonators for electron spin resonance: Sensitivity analysis, design and construction methods, and potential applications, Mol Phys, 111 (2013) 2674-2682.

[17] Y. Twig, E. Dikarov, W.D. Hutchison, A. Blank, Note: High sensitivity pulsed electron spin resonance spectroscopy with induction detection, Rev Sci Instrum, 82 (2011) 076105.

[18] Y. Twig, E. Dikarov, A. Blank, Cryogenic electron spin resonance microimaging probe, J Magn Reson, 218 (2012) 22-29.

[19] Y. Artzi, Y. Twig, A. Blank, Induction-detection electron spin resonance with spin sensitivity of a few tens of spins, Appl Phys Lett, 106 (2015) 084104.

[20] O.W.B. Benningshof, H.R. Mohebbi, I.A.J. Taminiau, G.X. Miao, D.G. Cory, Superconducting microstrip resonator for pulsed ESR of thin films, J Magn Reson, 230 (2013) 84-87.

[21] H. Malissa, D.I. Schuster, A.M. Tyryshkin, A.A. Houck, S.A. Lyon, Superconducting coplanar waveguide resonators for low temperature pulsed electron spin resonance spectroscopy, Rev Sci Instrum, 84 (2013) 025116.

[22] A.J. Sigillito, H. Malissa, A.M. Tyryshkin, H. Riemann, N.V. Abrosimov, P. Becker, H.-J. Pohl, M.L. Thewalt, K.M. Itoh, J.J. Morton, Fast, low-power manipulation of spin ensembles in superconducting microresonators, Appl Phys Lett, 104 (2014) 222407.

[23] P. Haikka, Y. Kubo, A. Bienfait, P. Bertet, K. Moelmer, Proposal for detection of a single electron spin in a microwave resonator, arXiv preprint arXiv:1609.01132, (2016).

[24] A. Bienfait, J.J. Pla, Y. Kubo, X. Zhou, M. Stern, C.C. Lo, C.D. Weis, T. Schenkel, D. Vion, D. Esteve, J.J.L. Morton, P. Bertet, Controlling spin relaxation with a cavity, Nature, 531 (2016) 74-77.

[25] C. Eichler, A. Sigillito, S. Lyon, J. Petta, Electron Spin Resonance at the Level of 10000 Spins Using Low Impedance Superconducting Resonators, arXiv preprint arXiv:1608.05130, (2016).

[26] D. Rugar, R. Budakian, H. Mamin, B. Chui, Single spin detection by magnetic resonance force microscopy, Nature, 430 (2004) 329-332.

[27] M.S. Grinolds, WarnerM, K. De Greve, DovzhenkoY, ThielL, R.L. Walsworth, HongS, MaletinskyP, YacobyA, Subnanometre resolution in three-dimensional magnetic resonance imaging of individual dark spins, Nat Nano, 9 (2014) 279-284.
[28] S. Baumann, W. Paul, T. Choi, C.P. Lutz, A. Ardavan, A.J. Heinrich, Electron paramagnetic resonance of individual atoms on a surface, Science, 350 (2015) 417-420.
[29] E.J. Reijerse, High-Frequency EPR Instrumentation, Appl Magn Reson, 37 (2010) 795-818.
[30] K.L. Nagy, D. Quintavalle, T. Feher, A. Janossy, Multipurpose High-Frequency ESR Spectrometer for Condensed Matter Research, Appl Magn Reson, 40 (2011) 47-63.
[31] C. Caspers, P.F. da Silva, M. Soundararajan, M.A. Haider, J.-P. Ansermet, Field and frequency modulated sub-THz electron spin resonance spectrometer, APL Photonics, 1 (2016) 026101.
[32] M. Bennati, T.F. Prisner, New developments in high field electron paramagnetic resonance with applications in structural biology, Reports on Progress in Physics, 68 (2005) 411.
[33] G.W. Morley, L.-C. Brunel, J. van Tol, A multifrequency high-field pulsed electron paramagnetic resonance/electron-nuclear double resonance spectrometer, Rev Sci Instrum, 79 (2008) 064703.
[34] J.D. Jackson, Classical electrodynamics, Third ed., Wiley, New York etc., 1999.
[35] D.J. Griffiths, Introduction to electrodynamics, 4th ed., Pearson, Boston, 2014.
[36] B. Razavi, A 300-GHz Fundamental Oscillator in 65-nm CMOS Technology, Ieee J Solid-St Circ, 46 (2011) 894-903.
[37] B. Razavi, RF microelectronics, 2nd, international ed., Pearson Education International, Upper Saddle River, NJ, 2012.
[38] S. Levantino, C. Samori, A. Bonfanti, S.L.J. Gierkink, A.L. Lacaita, V. Boccuzzi, Frequency dependence on bias current in 5 GHz CMOS VCOs: impact on tuning range and flicker noise upconversion, Ieee J Solid-St Circ, 37 (2002) 1003-1011.
[39] P. Kinget, Amplitude detection inside CMOS LC oscillators, Ieee Int Symp Circ S, (2006) 5147-5150.
[40] J.P. Goldsborough, M. Mandel, G.E. Pake, Influence of Exchange Interaction on Paramagnetic Relaxation Times, Phys Rev Lett, 4 (1960) 13-15.
[41] D.G. Mitchell, R.W. Quine, M. Tseitlin, R.T. Weber, V. Meyer, A. Avery, S.S. Eaton, G.R. Eaton, Electron Spin Relaxation and Heterogeneity of the 1:1 α,γ-Bisdiphenylene-β-phenylallyl (BDPA)/Benzene Complex, The Journal of Physical Chemistry B, 115 (2011) 7986-7990.
[42] N. Azuma, T. Ozawa, J. Yamauchi, Molecular and Crystal Structures of Complexes of Stable Free Radical BDPA with Benzene and Acetone, Bulletin of the Chemical Society of Japan, 67 (1994) 31-38.
[43] J.S. Thorp, A.R. Skinner, The Dependence of EPR Linewidth on Concentration in Mn/Mgo Single Crystals, J Magn Magn Mater, 69 (1987) 34-42.
[44] T. Phan, P. Zhang, H. Tran, S. Yu, Electron spin resonance study of Mn-doped metal oxides annealed at different temperatures, Journal of the Korean Physical Society, 57 (2010) 1270-1276.
[45] E. Ohmichi, Y. Tokuda, R. Tabuse, D. Tsubokura, T. Okamoto, H. Ohta, Multi-frequency force-detected electron spin resonance in the millimeter-wave region up to 150 GHz, Rev Sci Instrum, 87 (2016) 073904.
[46] S. Haravifard, D. Graf, A.E. Feiguin, C.D. Batista, J.C. Lang, D.M. Silevitch, G. Srajer, B.D. Gaulin, H.A. Dabkowska, T.F. Rosenbaum, Crystallization of spin superlattices with pressure and field in the layered magnet SrCu2(BO3)2, Nat Commun, 7 (2016).
[47] M.E. Zayed, C. Rüegg, T. Strässle, U. Stuhr, B. Roessli, M. Ay, J. Mesot, P. Link, E. Pomjakushina, M. Stingaciu, K. Conder, H.M. Rønnow, Correlated Decay of Triplet Excitations in the Shastry-Sutherland Compound SrCu2(B03)2, Phys Rev Lett, 113 (2014) 067201.
[48] P. Kuppusamy, P.T. Manoharan, Exchange Interactions in Bis(Tetramethylammonium) Bis(Maleonitriledithiolato)Cuprate(Ii), [Nme4]2[Cu(Mnt)2] - a Quasi-1-D Weak-Exchange System, Inorg Chem, 24 (1985) 3053-3057.
[49] W. Steyaert, P. Reynaert, A 0.54 THz Signal Generator in 40 nm Bulk CMOS With 22 GHz Tuning Range and Integrated Planar Antenna, Ieee J Solid-St Circ, 49 (2014) 1617-1626.
[50] M. Seo, M. Urteaga, J. Hacker, A. Young, Z. Griffith, V. Jain, R. Pierson, P. Rowell, A. Skalare, A. Peralta, InP HBT IC technology for terahertz frequencies: Fundamental oscillators up to 0.57 THz, Ieee J Solid-St Circ, 46 (2011) 2203-2214.
[51] A. Hajimiri, T.H. Lee, The design of low noise oscillators, 2nd ed., Kluwer Academic Publisher, Boston, 2000.
[52] A. Hajimiri, T.H. Lee, A general theory of phase noise in electrical oscillators, Ieee J Solid-St Circ, 33 (1998) 179-194.
[53] T.H. Lee, A. Hajimiri, Oscillator phase noise: a tutorial, Ieee J Solid-St Circ, 35 (2000) 326-336.
[54] M. Shahmohammadi, M. Babaie, R.B. Staszewski, A 1/f Noise Upconversion Reduction Technique for Voltage-Biased RF CMOS Oscillators, Ieee J Solid-St Circ, 51 (2016) 2610-2624.
[55] M. Grisi, G. Gualco, G. Boero, A broadband single-chip transceiver for multi-nuclear NMR probes, Rev Sci Instrum, 86 (2015).